JM PAPERS

Gill's stability problem may be unstable with horizontal heterogeneity in permeability

B.M. Shankar[1,†] **and I.S. Shivakumara**[2]

[1]Department of Mathematics, PES University, Bangalore 560 085, India
[2]Department of Mathematics, Bangalore University, Bangalore 560 056, India

The linear stability of thermal buoyant flow in a fluid-saturated vertical porous slab is studied under the assumption of weak and strong horizontal heterogeneities of the permeability. The two end vertical isothermal boundaries are impermeable and some paradigmatic cases of linear, quadratic and exponential heterogeneity models are deliberated. The stability/instability of the basic flow is examined by carrying out a numerical solution of the governing equations for the disturbances as Gill's proof (A.E. Gill, *J. Fluid Mech*, vol. 35, 1969, pp. 545–547) of linear stability is found to be ineffective. The possibilities of base flow becoming unstable due to heterogeneity in permeability are recognized, in contrast to Gill's stability problem. The neutral stability curves are presented and the critical Darcy–Rayleigh number for the onset of convective instability is computed for different values of the variable permeability constant. The similarities and differences between different heterogeneity models on the stability of fluid flow are clearly discerned.

Key words: Buoyancy-driven instability, convection in porous media

1. Introduction

Over the last few decades, considerable research efforts have been devoted to studying the stability of natural convection in a vertical porous slab because of its applications in the analysis of contaminant diffusion in the soil, the extraction of hydrocarbons, the CO_2 sequestration processes, the use of metal foams for the optimized design of heat exchangers, the design of packed bed reactors, building insulation involving an unventilated air gap and for breathing walls to chemical engineering to mention a few.

The first proof that a vertical porous slab of Darcy type with constant permeability, which is held at fixed but different temperatures on the impermeable vertical walls, is stable to perturbations from the equilibrium state was presented by Gill (1969).

† Email address for correspondence: bmshankar@pes.edu

Subsequently, several articles were dealt with other extensions on Gill's problem (Wolanski 1973; Rees 1988, 2011; Straughan 1988; Flavin & Rionero 1999; Scott & Straughan 2013; Barletta & De B. Alves 2014). All these studies revealed that no instability is possible in the sense that the basic solution is always linearly stable to two-dimensional disturbances no matter how large the Darcy–Rayleigh number is and thus complemented the results of Gill (1969). The state-of-the-art has been summarized in a monograph by Nield & Bejan (2017).

The proof of stability drawn in Gill's paper is shown to be ineffective if the vertical boundaries are considered as permeable instead of impermeable and it was also displayed that the basic state becomes unstable when the Darcy–Rayleigh number is larger than 197.081 (Barletta 2015). This work motivated many investigators to extend the study by including other effects such as an internal heat source (Barletta 2016; Barletta & Celli 2017), local thermal non-equilibrium (Celli, Barletta & Rees 2017) and anisotropy (Barletta & Celli 2021). Furthermore, the problem of Gill was analysed for an Oldroyd-B type of viscoelastic fluid (Shankar & Shivakumara 2017), Brinkman model (Shankar, Kumar & Shivakumara 2017), maximum density effect (Naveen, Shankar & Shivakumara 2020), second diffusing component (Shankar, Naveen & Shivakumara 2022) and the possibility of the basic flow becoming unstable was established in all these cases.

Another important topic that has attracted the attention of researchers in recent years is the study of thermal convective instability in a heterogeneous porous medium. This is because the permeability of the porous materials encountered in many practical situations is heterogeneous, such as the artificial porous materials like pellets used in chemical engineering processes, fibre material used for the insulating purposes and in many geological systems. It is shown experimentally that the porosity near a solid wall is not a constant but varies, due to which the permeability also varies (Schwartz & Smith 1953, Roblee, Baird & Tierney 1958; Benenati & Brosilow 1962). Since then, the significance and importance of heterogeneity for various aspects of convection in porous media have been continued to be recognized by scientists and engineers. The study of natural convection in horizontal porous media with variable permeability has been studied extensively (Nield & Kuznetsov 2007; Nield 2008; Rionero 2011; Barletta, Celli & Kuznetsov 2012; Barletta & Nield 2012). It has been observed that the effect of heterogeneity of the permeability has a noticeable impact in promoting the onset of instability.

On the other hand, Braester & Vadasz (1993) considered the effect of the general form of stratification of the porous-medium permeability and thermal conductivity on natural convection and showed that weak heterogeneity in permeability plays a relatively passive role. Rees & Pop (2000) studied the effect of exponentially decaying permeability on free convective boundary-layer flow induced by a vertical heated surface embedded in a porous medium and held at a constant temperature. It was found that, near the leading edge, the flow is enhanced and the rate of heat transfer is much higher than in the uniform permeability case. The effect of spatial discretization and different types of heterogeneous hydraulic conductivity fields on free thermal convection was examined by Nguyen, Graf & Guevara Morel (2016). The global sensitivity analysis and uncertainty quantification were used to study natural convection in heterogeneous porous media, including velocity-dependent dispersion by Fajraoui *et al.* (2017). Salibindla *et al.* (2018) conducted an experimental investigation of the dissolution convection in a porous medium with multiscale heterogeneity and some important implications for the future estimation of subsurface carbon sequestration were presented. Shafabakhsh *et al.* (2019) considered the influence of a fractured heterogeneity effect on unstable density-driven flow. It was

shown that the onset of instability and free convection occur with a lower critical Rayleigh number, indicating the fractured networks have a destabilizing effect. Benham, Bickle & Neufeld (2021) studied the effect of vertical heterogeneity in a porous medium on the overall flow properties by way of upscaling and illustrated how and when heterogeneities accelerate/decelerate the dynamic flow. The effect of permeability variation on natural convection in a vertical porous layer subjected to constant heat fluxes along the sidewalls was investigated by Damene *et al.* (2021). The results for the flow field, temperature distribution and heat transfer rates were presented for various forms of the variable permeability cases.

As envisaged by the previous studies, flows in porous media are particular in that the velocity field and heat transfer are largely dictated by the medium properties. Practically every porous domain exhibits heterogeneity with respect to permeability. It is thus imperative to establish the implications of horizontal heterogeneities in controlling the onset, growth and/or decay of thermal instabilities in a vertical porous layer, which have not received any attention to the best of our knowledge. The intent of the present study is to quantify the effect of both weak and strong heterogeneities of the permeability on the stability of natural convection in a vertical Darcy porous layer. In the discussion, three different models of permeability functions are considered viz. linear, quadratic and exponential. The stability of basic parallel buoyant flow for these models is analysed by adopting a modal analysis. The stability eigenvalue problem is solved numerically by employing the Chebyshev collocation method. The effects of different models of heterogeneities on the stability/instability characteristics are discussed for the neutral stability curves and for the critical values of the Darcy–Rayleigh number, wavenumber and wave speed.

2. Mathematical formulation

An infinite vertical porous slab of width $2h$ saturated with an incompressible Newtonian fluid and bounded by a pair of impermeable left ($x^* = -h$) and right ($x^* = h$) vertical walls which are maintained at constant temperatures T_1 and $T_2(> T_1)$, respectively is considered (see figure 1). The origin of the coordinate axes is taken in the middle of the slab with the z^*-axis pointing vertically upward and the gravitational acceleration $\boldsymbol{g}$ is acting in the negative z^* direction, while the x^*- and y^*-axes are horizontal. The flow in the Darcy porous medium is driven by the buoyancy force due to the temperature difference between the vertical walls. The local thermodynamic equilibrium and the Oberbeck–Boussinesq approximation are assumed. Besides, the permeability of the porous medium is assumed to vary horizontally within the porous medium. With asterisks being used to denote the dimensional variables, the governing equations describing the system behaviour are

$$\nabla^* \cdot \boldsymbol{u}^* = 0, \tag{2.1}$$

$$-\nabla^* P^* + \rho_0 \beta (T^* - T_0) g \hat{k} - \frac{\mu}{K^*(x^*)} \boldsymbol{u}^* = 0, \tag{2.2}$$

$$\chi \frac{\partial T^*}{\partial t^*} + (\boldsymbol{u}^* \cdot \nabla^*) T^* = \kappa \nabla^{*2} T^*. \tag{2.3}$$

In the above equations, $\boldsymbol{u}^* = (u^*, v^*, w^*)$ is the filtration velocity, P^* is the pressure, ρ_0 is the density at the reference temperature $T_0 = (T_1 + T_2)/2$, β is the volumetric thermal expansion coefficient, T^* is the temperature, μ is the viscosity of the fluid, $K^*(x^*)$ is the
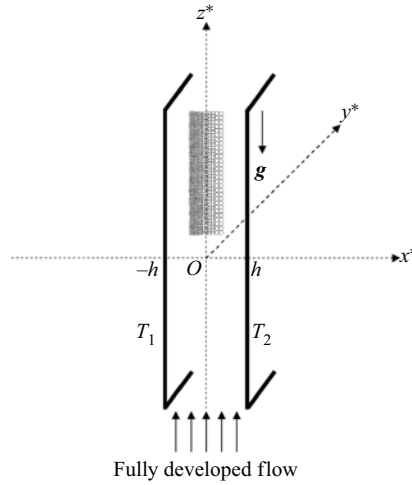
Figure 1. Physical configuration.

horizontally varying permeability function, χ is the ratio of heat capacities and κ is the thermal diffusivity.

The boundary conditions are:

$$u^* = 0 \text{ at } x^* = \pm h; \quad T^* = T_1 \text{ at } x^* = -h; \quad T^* = T_2 \text{ at } x^* = h. \qquad (2.4a\text{--}c)$$

We non-dimensionalize the above equations through the transformation

$$\nabla = h\nabla^*, \quad \boldsymbol{u} = \frac{\boldsymbol{u}^*}{(\kappa/h)}, \quad P = \frac{P^*}{(\mu\kappa/K_0)}, \quad t = \frac{t^*}{(\chi h^2/\kappa)}.$$

$$T = \frac{(T^* - T_0)}{(T_2 - T_1)}, \quad K(x) = \frac{K^*(x^*)}{K_0}, \qquad\qquad (2.5\, a\text{--}f)$$

where K_0 is a reference permeability at the centre of the porous slab. In analysing instability problems akin to the present investigation, Barletta (2015), Barletta, Celli & Ouarzazi (2017) and Shankar, Shivakumara & Naveen (2021) have established the validity of Squire's theorem (i.e. two-dimensional disturbances are more unstable than the three-dimensional ones). Motivated by these findings, we have restricted our attention purely to two-dimensional analysis and accordingly the streamfunction $\psi^*(x^*, z^*, t^*)$ is introduced through $u^* = \partial\psi^*/\partial z^*$ and $w^* = -\partial\psi^*/\partial x^*$. The pressure term is then eliminated from the momentum equation by operating curl and the following dimensionless equations are obtained:

$$\frac{1}{K(x)}\nabla^2\psi - \frac{DK(x)}{[K(x)]^2}\frac{\partial\psi}{\partial x} = -R_D\frac{\partial T}{\partial x}, \qquad (2.6)$$

$$\frac{\partial T}{\partial t} - J(\psi, T) = \nabla^2 T, \qquad (2.7)$$

where D denotes the derivative with respect to x, $R_D = \beta g h K_0(T_2 - T_1)/\nu\kappa$ is the Darcy–Rayleigh number, $J(\psi, T) = (\partial\psi/\partial x)(\partial T/\partial z) - (\partial\psi/\partial z)(\partial T/\partial x)$ is the Jacobian and $\nu = \mu/\rho_0$ is the kinematic viscosity.

943 A20-4

The boundary conditions now become

$$\psi = 0 \text{ at } x = \pm 1 \quad \text{and} \quad T = \pm\tfrac{1}{2} \text{ at } x = \pm 1. \tag{2.8a,b}$$

It is convenient to introduce the following modified Darcy–Rayleigh number based on the average permeability $\bar{K}(x)$ as $\tilde{R}_D = \beta g h \bar{K}(x)(T_2 - T_1)/\nu\kappa$, where $\bar{K}(x) = bK_0$ with

$$b = \frac{1}{2} \int_{-1}^{1} K(x)\, dx. \tag{2.9}$$

The Darcy–Rayleigh number is related to the modified Darcy–Rayleigh number $\tilde{R}_D$ by the following expression:

$$\tilde{R}_D = bR_D. \tag{2.10}$$

Natural and man-made porous domains exhibit heterogeneity in permeability and it can vary by many orders of magnitude and sometimes rapidly over small spatial scales. As such, the prediction of weak and strong heterogeneities in controlling the growth and/or decay of instabilities may turn out to be important in many of the engineering applications mentioned earlier. Accordingly, the following heterogeneity models, with m being the variable permeability constant, are considered:

Linear heterogeneity of the permeability

$$K(x) = 1 + mx; \quad b = 1. \tag{2.11}$$

Quadratic heterogeneity of the permeability

$$K(x) = 1 + mx^2; \quad b = 1 + m/3. \tag{2.12}$$

Exponential heterogeneity of the permeability

$$K(x) = e^{mx}; \quad b = \sinh m/m. \tag{2.13}$$

3. Base state

The base state, about which the linear stability characteristics will be analysed, corresponds to a steady, parallel, fully developed flow. Base state quantities are designated by suffix b, and also ψ_b and T_b are considered to be functions of x alone. Equations (2.6)–(2.8a,b), respectively become

$$\frac{1}{K(x)} D^2 \psi_b - \frac{DK(x)}{[K(x)]^2} D\psi_b = -\frac{\tilde{R}_D}{b} DT_b, \tag{3.1}$$

$$D^2 T_b = 0, \tag{3.2}$$

$$\psi_b = 0 \text{ at } x = \pm 1 \quad \text{and} \quad T_b = \pm\tfrac{1}{2} \text{ at } x = \pm 1. \tag{3.3a,b}$$

The solutions of the above equations obtained analytically for linear, quadratic and exponential heterogeneities of the permeability are, respectively, given by

$$\psi_b(x) = \frac{\tilde{R}_D}{12}[m^2 - 2mx - 3](x^2 - 1), \quad T_b = \frac{x}{2}. \tag{3.4a,b}$$

$$\psi_b(x) = -\frac{\tilde{R}_D}{8(1 + m/3)}[m(x^2 + 1) + 2](x^2 - 1), \quad T_b = \frac{x}{2}. \tag{3.5a,b}$$

$$\psi_b(x) = \frac{\tilde{R}_D}{4\sinh m}[-2\,\mathrm{e}^m - \mathrm{e}^{m(x+2)}(x-1) + \mathrm{e}^{mx}(x+1)](\coth m - 1), \quad T_b = \frac{x}{2}.$$

$$(3.6a,b)$$

One may easily check that the basic solution given by (3.4a,b)–(3.6a,b) coincides with that of Gill (1969) when $m = 0$ (constant permeability). Equations (3.4a,b)–(3.6a,b) reveal that $\psi_b(x)$ is not symmetric about the z-axis for linear and exponential, while it is symmetric for quadratic heterogeneities of the permeability. Moreover, $\psi_b(x)/\tilde{R}_D$ remains invariant under the transformation

$$m \to -m, \quad x \to -x,$$

$$(3.7a,b)$$

for linear and exponential heterogeneities of the permeability.

4. Linear stability analysis

We perturb the basic state with small-amplitude disturbances given by

$$\psi = \psi_b + \varepsilon\hat{\psi}, \quad T = T_b + \varepsilon\hat{T},$$

$$(4.1a,b)$$

where the parameter ε is such that $\varepsilon > 0$ and $\varepsilon \ll 1$, while $\hat{\psi}$ and $\hat{T}$ are the perturbation fields. We assume the perturbed streamfunction and temperature have the form of normal modes

$$(\hat{\psi}, \hat{T})(x, z, t) = (\Psi, \Theta)(x)\,\mathrm{e}^{ia(z-ct)},$$

$$(4.2)$$

where a is the vertical wavenumber and $c = c_r + ic_i$ is the complex wave speed. The growth rate c_i marks the difference between stability ($c_i < 0$) and instability ($c_i > 0$). The neutrally stable configuration is identified by $c_i = 0$. Substituting equations (4.1a,b) and (4.2) into (2.6)–(2.8a,b), we obtain the following eigenvalue problem for neutrally stable modes:

$$\frac{1}{K(x)}(D^2 - a^2)\Psi - \frac{DK(x)}{[K(x)]^2}D\Psi + \frac{\tilde{R}_D}{b}D\Theta = 0,$$

$$(4.3)$$

$$ia(\tfrac{1}{2}\Psi - D\psi_b\Theta) - (D^2 - a^2)\Theta = iac\Theta,$$

$$(4.4)$$

$$\Psi = \Theta = 0 \text{ at } x = \pm1.$$

$$(4.5)$$

We note that the above eigenvalue problem is endowed with symmetry if $K(x)$ varies linearly and exponentially, and in which cases (4.3)–(4.5) are left invariant by the transformation

$$\Psi \to -\Psi, \quad x \to -x, \quad m \to -m, \quad a \to -a, \quad c \to -c.$$

$$(4.6a–e)$$

5. Gill's growth rate analysis

It is not out of place to attempt to determine whether Gill's proof of linear stability for constant permeability can be extended to the cases of horizontal heterogeneity models of the permeability. Following the analysis of Gill (1969), we operate $(1/K(x))(D^2 - a^2) - (DK(x)/[K(x)]^2)D$ on (4.4) to eliminate Ψ and obtain a single fourth-order differential

equation for Θ in the form

$$
\begin{aligned}
-\frac{ia\tilde{R}_D}{2b}\Theta' - ia\Bigg\{ &\frac{1}{K(x)}(\psi'''{}_b\Theta + 2\psi''{}_b\Theta' + \psi'{}_b\Theta'' \\
&- a^2\psi'{}_b\Theta) - \frac{K'(x)}{[K(x)]^2}(\psi''{}_b\Theta + \psi'{}_b\Theta')\Bigg\} \\
-\frac{1}{K(x)}(\Theta'''' + a^4\Theta - 2a^2\Theta'') &+ \frac{K'(x)}{[K(x)]^2}(\Theta''' - a^2\Theta') \\
= iac\Bigg\{\frac{1}{K(x)}(\Theta'' - a^2\Theta) &- \frac{K'(x)}{[K(x)]^2}\Theta'\Bigg\},
\end{aligned}
\tag{5.1}
$$

where primes denote differentiation with respect to x. We multiply equation (5.1) by $\bar{\Theta}$, the complex conjugate of Θ, and integrate it over the domain $-1 \le x \le 1$ to get

$$
\begin{aligned}
-\frac{ia\tilde{R}_D}{2b}\int_{-1}^{1}\Theta'\bar{\Theta}\,\mathrm{d}x &- ia\int_{-1}^{1}\Bigg\{\frac{1}{K(x)}(\psi'''{}_b|\Theta|^2 + 2\psi''{}_b\Theta'\bar{\Theta} + \psi'{}_b\Theta''\bar{\Theta} - a^2\psi'{}_b|\Theta|^2) \\
&- \frac{K'(x)}{[K(x)]^2}(\psi''{}_b|\Theta|^2 + \psi'{}_b\Theta'\bar{\Theta})\Bigg\}\,\mathrm{d}x \\
-\int_{-1}^{1}\Bigg\{\frac{1}{K(x)}(\Theta''''\bar{\Theta} + a^4|\Theta|^2 &- 2a^2\Theta''\bar{\Theta}) - \frac{K'(x)}{[K(x)]^2}(\Theta'''\bar{\Theta} - a^2\Theta'\bar{\Theta})\Bigg\}\,\mathrm{d}x \\
= iac\int_{-1}^{1}\Bigg\{\frac{1}{K(x)}(\Theta''\bar{\Theta} - a^2|\Theta|^2) &- \frac{K'(x)}{[K(x)]^2}\Theta'\bar{\Theta}\Bigg\}\,\mathrm{d}x.
\end{aligned}
\tag{5.2}
$$

The terms in (5.2) rule out the possibility of reaching any definite conclusion in determining whether the sign of c_i is positive or negative. Hence, Gill's analysis of proving the stability becomes ineffective owing to the consideration of horizontal heterogeneity of the permeability. However, for a constant permeability case ($K(x) = 1$, $\tilde{R}_D = R_D$ with $b = 1$, $\psi_b = \psi_b(x) = R_D(1 - x^2)/4$) the above equation simply reduces to

$$
\begin{aligned}
\frac{iaR_D}{2}\int_{-1}^{1}x(|\Theta'|^2 + a^2|\Theta|^2)\,\mathrm{d}x &+ \int_{-1}^{1}(|\Theta''|^2 + a^4|\Theta|^2 \\
+ 2a^2|\Theta'|^2)\,\mathrm{d}x &= iac\int_{-1}^{1}(|\Theta'|^2 + a^2|\Theta|^2)\,\mathrm{d}x.
\end{aligned}
\tag{5.3}
$$

Equating the real part of (5.3) allows one to conclude that $c_i < 0$, indicating that all infinitesimal perturbations decay. This conclusion is in conformity with Gill's classical proof of stability.

6. Numerical procedure

The ensued eigenvalue problem formulated through (4.3)–(4.5) is solved numerically by means of the Chebyshev collocation method as Gill's analysis is ineffective in establishing the stability/instability of the base flow. The Chebyshev polynomial of kth order is given by

$$
\xi_k(x) = \cos k\theta, \quad \theta = \cos^{-1}x.
\tag{6.1}
$$

The Chebyshev collocation points are given by

$$
x_j = \cos\left(\frac{\pi j}{N}\right), \quad j = 0(1)N,
\tag{6.2}
$$

where N is any positive integer and $j = 0$ and $j = N$ correspond to the right and left wall boundaries, respectively. The field variables Ψ and Θ are approximated in terms of Chebyshev polynomials as

$$\Psi(x) = \sum_{j=0}^{N} \Psi_j \xi_j(x), \quad \Theta(x) = \sum_{j=0}^{N} \Theta_j \xi_j(x), \qquad (6.3a,b)$$

where Ψ_j and Θ_j are constants. Equations (4.3)–(4.5) are discretized in terms of Chebyshev polynomials to get

$$\frac{1}{K(x_j)} \sum_{k=0}^{N} (B_{jk}\Psi_k - a^2\Psi_j) - \frac{K'(x_j)}{[K(x_j)]^2} \sum_{k=0}^{N} A_{jk}\Psi_k + \frac{\tilde{R}_D}{b} \sum_{k=0}^{N} A_{jk}\Theta_k = 0, \quad j = 1(1)N - 1,$$
$$(6.4)$$

$$\frac{ia}{2}\Psi_j - ia\psi'_{b_j}\Theta_j - \left(\sum_{k=0}^{N} B_{jk}\Theta_k - a^2\Theta_j\right) = iac\Theta_j, \quad j = 1(1)N - 1, \qquad (6.5)$$

$$\Psi_0 = \Psi_N = 0, \qquad (6.6)$$

$$\Theta_0 = \Theta_N = 0, \qquad (6.7)$$

where

$$A_{jk} = \begin{cases} \dfrac{c_j(-1)^{k+j}}{c_k(x_j - x_k)} & j \neq k \\ -\dfrac{x_j}{2(1 - x_j^2)} & 1 \leq j = k \leq N - 1 \\ \dfrac{2N^2 + 1}{6} & j = k = 0 \\ -\dfrac{2N^2 + 1}{6} & j = k = N \end{cases}, \qquad (6.8)$$

and

$$B_{jk} = A_{jm} \cdot A_{mk}, \qquad (6.9)$$

with

$$c_j = \begin{cases} 1 & 1 \leq j \leq N - 1 \\ 2 & j = 0, N \end{cases}. \qquad (6.10)$$

The discretized equations lead to a generalized eigenvalue problem of the form

$$\boldsymbol{AX} = c\boldsymbol{BX}, \qquad (6.11)$$

where c and $\boldsymbol{X}$ are the complex eigenvalue and eigenfunction, respectively, and $\boldsymbol{A}$ and $\boldsymbol{B}$ are square complex matrices of order $2N + 2$. The differential eigenvalue problem then becomes an algebraic eigenvalue problem that can be solved in different ways. In this study, the QZ algorithm is used to obtain the eigenvalues inbuilt in MATLAB software with the eig command. The imaginary part of the eigenvalue c is used to determine the critical value of parameter $\tilde{R}_D$ using criticality conditions of temporal linear stability analysis (Shankar, Kumar & Shivakumara 2020, 2021; Shankar & Shivakumara 2020, 2021).

7. Discussion of the results

This section examines the linear temporal stability results of fully developed natural convection flow in a differentially heated heterogeneous vertical porous slab. The effect of linear, quadratic and exponential heterogeneities of the permeability is discussed on the flow instability by searching for disturbances in the form of normal modes. The present study contains the following two important non-dimensional parameters: the modified Darcy–Rayleigh number ($\tilde{R}_D$) and the variable permeability constant (m).

7.1. *Base flow*

The scaled basic streamfunction $\psi_b(x)/\tilde{R}_D$ is plotted in figures 2(a), 2(b) and 2(c) for linear, quadratic and exponential heterogeneity models of the permeability, respectively, for different positive and negative values of m and note that the base flow is greatly affected. Figure 2(a) demonstrates that the basic streamfunction profile gets suppressed and starts showing an inflection point near the walls as the magnitude of m increases. Furthermore, the inflection points gradually move towards the centre of the slab from the cold and hot walls as the value of m and $-m$ increase, respectively. For the quadratic heterogeneity model, the basic streamfunction profiles are quartic functions that contain only even powers of x (figure 2b). In this case, the inflection points are found to appear only for negative values of m and move towards the z-axis with increasing $-m$. Moreover, the profiles attain some maximum value at the centreline of the porous slab and this value increases with increasing m but decreases with increasing $-m$. Figure 2(c) reveals that the exponentially varying permeability compresses the streamfunction profiles towards the hot wall as m increases while it moves in the direction of the cold wall as $-m$ increases. Besides, these profiles become steeper near the boundaries at higher values of $|m|$ and also exhibit inflection points. Figures 2(a) and 2(c) show the invariance of $\psi_b/\tilde{R}_D$ as visualized by (3.7a,b). The appearance of inflection points for various models of heterogeneity is linked to the instability of base flow.

7.2. *Validation of the code*

The convergence analysis of the numerical calculations is presented by varying the order of the Chebyshev polynomials for different forms of heterogeneity of the permeability function $K(x)$ and for various values of the variable permeability constant m in table 1. From the table, it is evident that the critical values of $\tilde{R}_D$ are independent of the order of polynomial N in the approximation of different field variables varying from 30 to 60. In particular, the numerical scheme needs a good number of collocation points as $m \to 0$; otherwise, $N = 30$ collocation points are found to be sufficient for achieving four decimal point accuracy. Due to the lack of benchmark solutions in the open literature with which to compare our results, numerical computations are also carried out using the Galerkin method with Legendre polynomials as trial functions (see Appendix A). The results achieved by both the Galerkin and Chebyshev collocation methods for different forms of $K(x)$ and m values are tabulated in table 2 and note that they are in good agreement.

7.3. *Growth rate analysis*

We could not find the analytical proof that the solution of (4.3)–(4.5) yields $c_i < 0$, as was found for a constant permeability case (Gill 1969). As a result, numerical computations of the complex eigenvalue c_i for the assigned values of a, $\tilde{R}_D$ and m which allow one
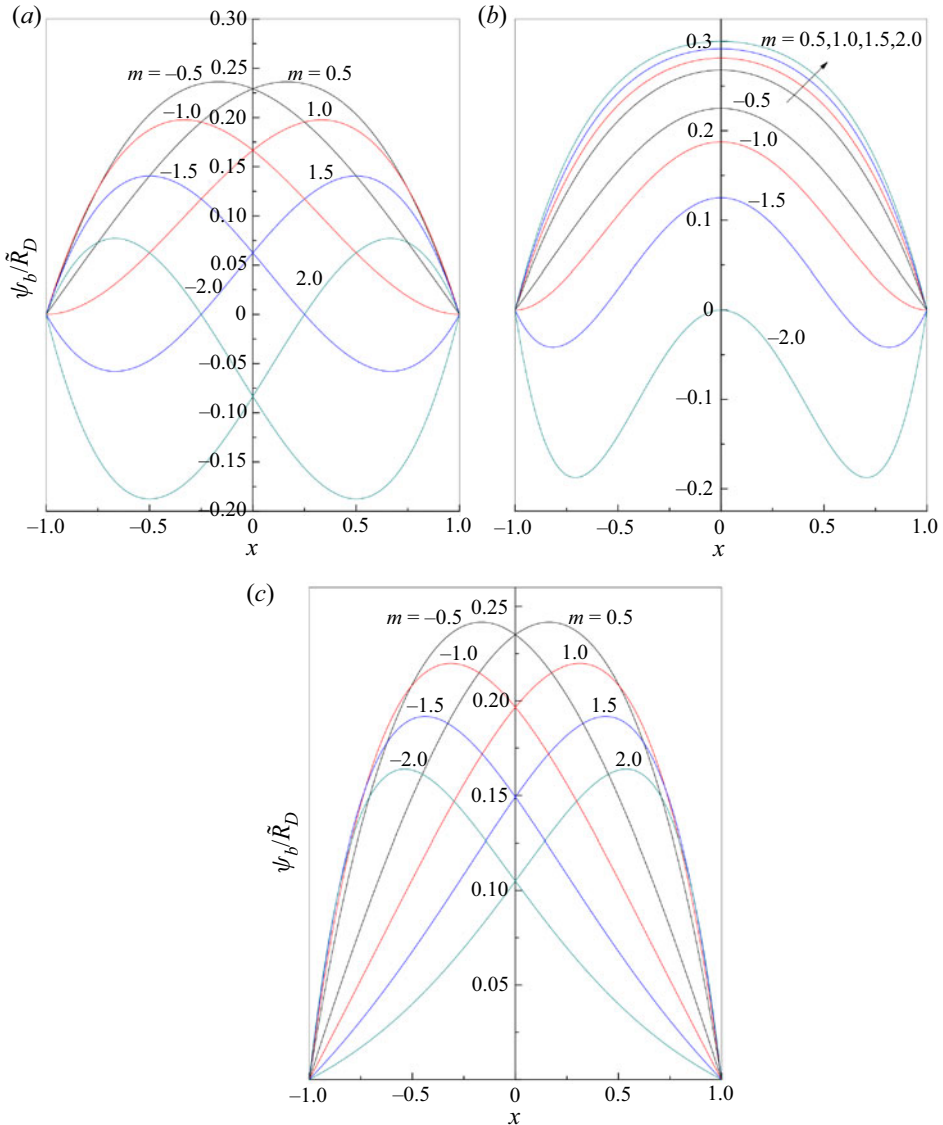
Figure 2. Plots of the scaled basic streamfunction profiles for different heterogeneity models of the permeability: (*a*) linear, (*b*) quadratic and (*c*) exponential.

to track the growth rate of the normal modes were taken up. The variation of c_i as a function of a is displayed in figures 3(*a*–*c*), 4(*a*–*c*) and 5(*a*–*c*) for linear, quadratic and exponential forms of $K(x)$, respectively, for different combinations of values of $\tilde{R}_D$ and m. These figures reveal the possibility of horizontal heterogeneities of the permeability instilling instability of the base flow depending on the values of $\tilde{R}_D$ and m. For the linear form of $K(x)$, the flow is always stable for all the considered values of $\tilde{R}_D$ when $|m| = 0.3$ (figure 3*a*). But the same cannot be said when $|m| = 0.4$ as the sign of c_i changes from negative to positive, for some values of $\tilde{R}_D$, indicating the possibility of the flow becoming unstable (figure 3*b*). The values of $|m|$ dominate in enforcing flow instability, as is evident from figure 3(*c*). Nonetheless, the positive and negative values of m alter the stability of

943 A20-10

Linear heterogeneity of the permeability

N	m = 0.4 $\tilde{R}_{Dc}$	a_c	c_c	m = 0.5 $\tilde{R}_{Dc}$	a_c	c_c	m = 0.6 $\tilde{R}_{Dc}$	a_c	c_c	m = 0.8 $\tilde{R}_{Dc}$	a_c	c_c
5												
10	21067.6456	1.9342	−6793.0898	1743.2398	2.0554	−489.1483	646.6506	1.1813	−155.8478	321.4857	1.7149	−71.6565
15	25598.4841	1.7350	−8280.6714	2003.4712	1.8170	−563.3863	767.6434	1.6258	−194.9108	329.1297	1.6605	−73.8798
20	31481.1216	1.4661	−10190.8083	1992.6862	1.9673	−560.9758	742.5172	1.9026	−188.9609	324.7345	1.6682	−72.8348
25	32605.8046	1.1293	−10526.8738	1991.9280	1.9702	−560.7680	742.1933	1.9198	−188.8929	324.7667	1.6677	−72.8429
30	32427.2357	1.1225	−10467.8322	1991.9150	1.9703	−560.7646	742.2006	1.9197	−188.8948	324.7667	1.6677	−72.8429
35	32424.8625	1.1282	−10467.6390	1991.9150	1.9703	−560.7646	742.2006	1.9197	−188.8948			
40	32425.9713	1.1277	−10467.9572									
45	32425.8891	1.1278	−10467.9325									
50	32425.8937	1.1278	−10467.9340									
55	32425.8937	1.1278	−10467.9340									

Quadratic heterogeneity of the permeability

N	m = −0.3 $\tilde{R}_{Dc}$	a_c	c_c	m = −0.4 $\tilde{R}_{Dc}$	a_c	c_c	m = −0.6 $\tilde{R}_{Dc}$	a_c	c_c	m = −0.8 $\tilde{R}_{Dc}$	a_c	c_c
5												
10	15243.9297	1.9550	±5652.3086	3183.5407	5.8311	±1099.9171	693.5232	3.2256	±210.4249	531.2256	1.2346	±128.1899
15	19781.3783	1.7447	±7376.3103	2980.4854	2.5985	±1017.9439	783.5181	2.8606	±237.9106	541.1062	2.6270	±153.0586
20	22796.9832	1.8841	±8532.0872	2862.4935	3.6574	±981.5656	785.5820	2.9738	±238.6966	496.4707	2.4772	±140.6779
25	22568.4981	2.4829	±8467.2544	2891.3574	3.6158	±991.5090	785.2343	2.9848	±238.5923	493.4203	2.4740	±139.7543
30	22228.0521	2.9889	±8352.2491	2889.0099	3.6209	±990.7038	785.2252	2.9851	±238.5895	493.4198	2.4741	±139.7542
35	22147.1881	3.1240	±8324.9195	2889.1313	3.6195	±990.7421	785.2252	2.9851	±238.5895	493.4198	2.4741	±139.7542
40	22139.3046	3.1621	±8322.8427	2889.1291	3.6196	±990.7417						
45	22139.8504	3.1672	±8323.1683	2889.1291	3.6196	±990.7416						
50	22140.0790	3.1668	±8323.2418									
55	22140.0729	3.1667	±8323.2419									
60	22140.0729	3.1667	±8323.2419									

Table 1. For caption see next page.

Exponential heterogeneity of the permeability

N	m = 0.6			m = 0.8			m = 2			m = 5		
	$\tilde{R}_{Dc}$	a_c	c_c	$\tilde{R}_{Dc}$	a_c	c_c	$\tilde{R}_{Dc}$	a_c	c_c	$\tilde{R}_{Dc}$	a_c	c_c
5	25020.1134	2.0199	−7292.9596	934.1515	0.9781	−215.0902	158.0176	1.3620	−22.8385	196.4047	2.1312	−15.4860
10	23609.5871	0.6220	−6755.9021	1120.8923	1.1491	−264.6928	175.3561	1.2686	−25.9780	520.6799	2.0378	−64.9447
15	23800.6598	0.7377	−6831.4736	1130.0910	1.2461	−267.4470	175.1173	1.2698	−25.9325	436.9794	2.5775	−57.0676
20	24038.4416	0.7127	−6897.0621	1130.7050	1.2448	−267.5947	175.1176	1.2698	−25.9326	434.5132	2.6026	−56.7344
25	24025.0718	0.7148	−6893.4743	1130.7046	1.2448	−267.5941	175.1176	1.2698	−25.9326	434.4402	2.6039	−56.7244
30	24025.2255	0.7147	−6893.5034	1130.7046	1.2448	−267.5941				434.4397	2.6039	−56.7243
35	24025.2371	0.7147	−6893.5068							434.4397	2.6039	−56.7243
40	24025.2370	0.7147	−6893.5068									
45	24025.2370	0.7147	−6893.5068									
50	24025.2370	0.7147	−6893.5068									

Table 1. Process of convergence of the Chebyshev collocation method for different values of variable permeability constant m.

$K(x)$	m	Chebyshev collocation method			Galerkin method		
		$\tilde{R}_{Dc}$	a_c	c_c	$\tilde{R}_{Dc}$	a_c	c_c
Linear	0.4	32425.8937	1.1278	-10467.9340	32425.8938	1.1278	-10467.9341
	0.6	742.2006	1.9197	-188.8948	742.2006	1.9197	-188.8948
	0.8	324.7667	1.6677	-72.8429	324.7667	1.6677	-72.8429
Quadratic	-0.3	22140.0729	3.1667	±8323.2419	22140.0730	3.1667	±8323.2419
	-0.5	1255.9550	3.2956	±402.1926	1255.9551	3.2956	±402.1927
	-0.8	493.4198	2.4741	±139.7542	493.4199	2.4741	±139.7543
Exponential	0.6	24025.2370	0.7147	-6893.5068	24025.2371	0.7145	-6893.5069
	2	175.1176	1.2698	-25.9326	175.1176	1.2698	-25.9326
	5	434.4397	2.6039	-56.7243	434.4398	2.6039	-56.7243

Table 2. Comparison of critical values computed by Chebyshev collocation and Galerkin methods.

the fluid flow if $K(x)$ varies quadratically (figure 4a–c). Figure 4(a) shows that the base flow is stable for all values of $\tilde{R}_D$ when $m = \pm0.2$. Whereas for $m = -0.3$ the chance of the flow becoming unstable cannot be ruled out as c_i changes its sign for some values of $\tilde{R}_D$ (figure 4b). The results presented for negative and positive values of m in figure 4(c) evidence some interesting facts. It is seen that the flow transition from stable to unstable occurs only for negative values of m, while the growth rate remains negative for all positive values of m, indicating the basic flow is stable according to linear stability analysis. This is expected as there is no inflection point in the basic streamfunction for the quadratic form of heterogeneity for values of $m \geq 0$. The results portrayed for the exponential form of $K(x)$ in figure 5(a–c) are similar to those of the linear form of $K(x)$ but the flow is found to be unstable at slightly higher values of $|m|$. Despite the flow becoming unstable at moderate values of $|m|$, it is noted that the base flow remains stable ($c_i < 0$) to disturbances of all wavenumbers for all values of the Darcy–Rayleigh number at lower values of $|m|$ and thus complement the results of constant permeability (Gill 1969).

7.4. *Neutral stability curves*

The transition to instability is described through the neutral stability curves in the $(a, \tilde{R}_D)$ parametric plane and such curves bound the instability region. Typically, instability occurs for values of $\tilde{R}_D$ larger than those lying above the neutral stability curve. Hence, the point of minimum $\tilde{R}_D$ at neutral stability is the endpoint for instability i.e. the instability arises within the region entrapped by the neutral stability curve. Hence, the minimum value of $\tilde{R}_D$ along each neutral stability curve defines the critical triplets $(a_c, \tilde{R}_{Dc}, c_c)$ which depend on the heterogeneity models and values of m. Instability is possible for $\tilde{R}_D > \tilde{R}_{Dc}$. Figures 6(a), 6(b) and 6(c), respectively, display the neutral stability curves for linear, quadratic and exponential forms of $K(x)$ for various values of m. For linear and exponential forms of the permeability functions, it is quite evident that the neutral stability curves exhibit a uni-modal shape and move upwards with decreasing $|m|$ and the same behaviour persists for the quadratic form of $K(x)$ but only for negative values of m. The linear (figure 6a) and quadratic (figure 6b) forms of $K(x)$ also demonstrate that the normal modes activating the instability correspond to decreasing wavenumber with increasing $|m|$ and $-m$, respectively, whereas a contradicting impact ensues when $K(x)$ varies exponentially (figure 6c).
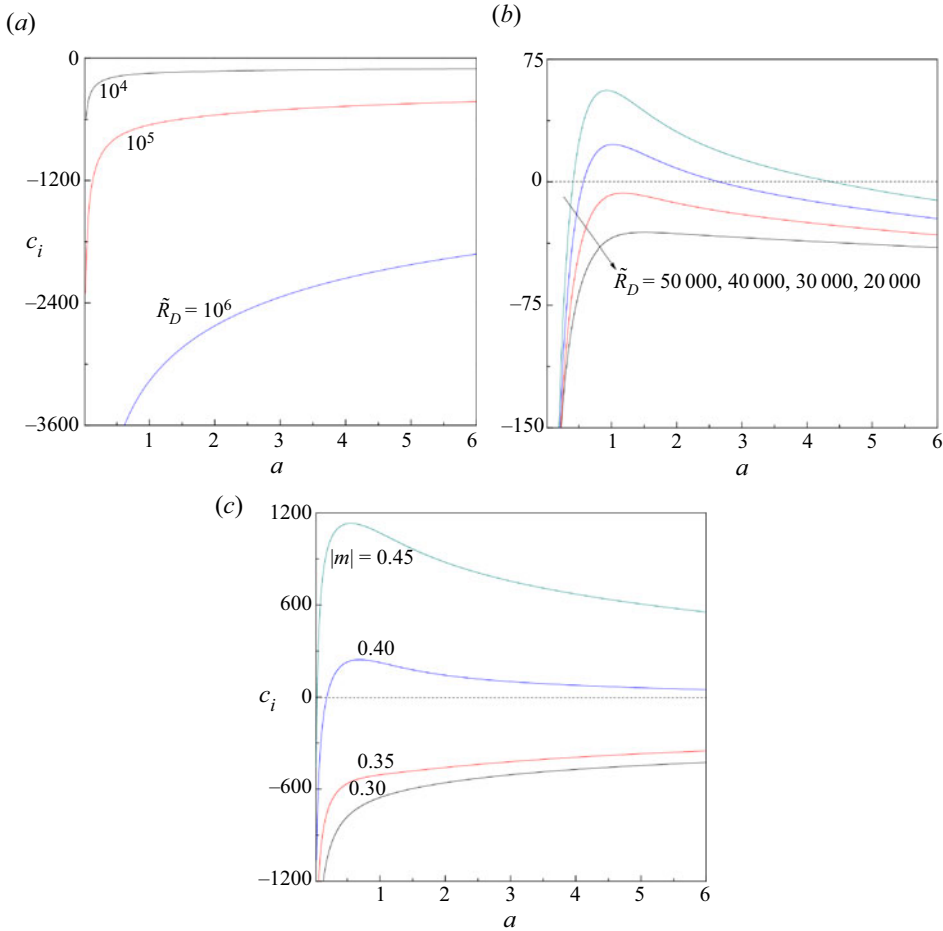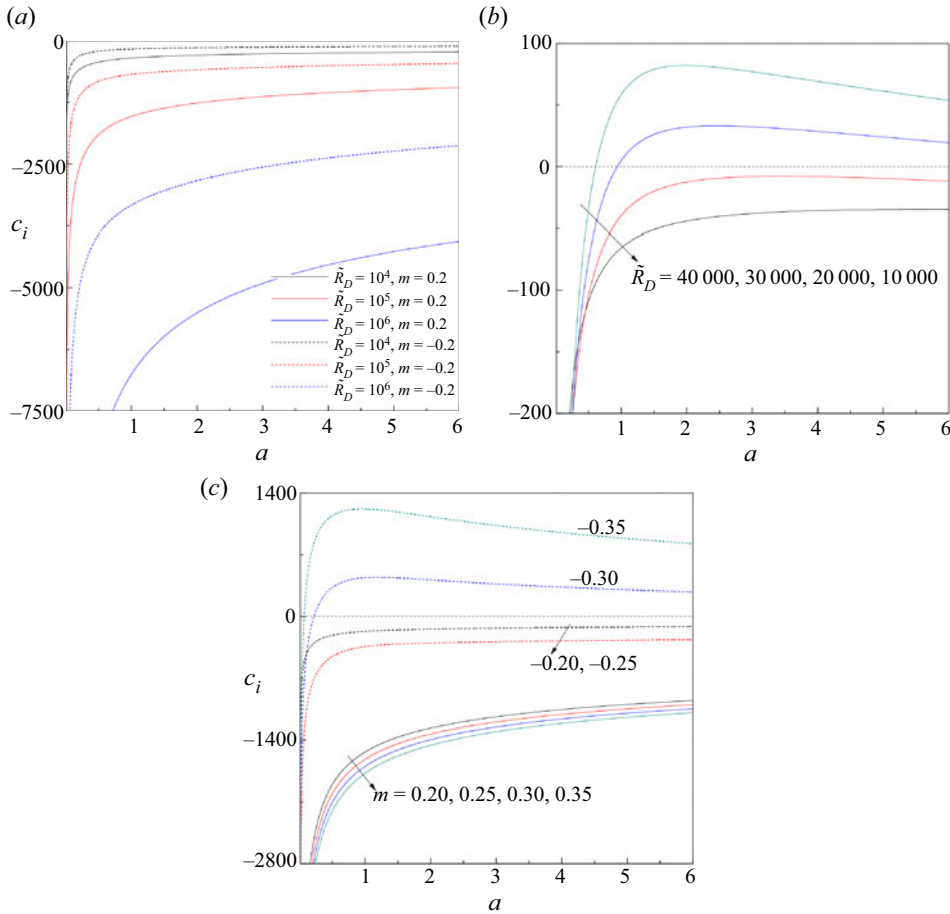
Figure 3. Growth rate c_i versus wavenumber a for different values of (a) $\tilde{R}_D$ with $|m| = 0.3$, (b) $\tilde{R}_D$ with $|m| = 0.4$ and (c) $|m|$ with $\tilde{R}_D = 10^5$ for a linear heterogeneity of the permeability.

7.5. *Linear stability boundaries*

The plots of $\tilde{R}_{Dc}$, a_c and c_c are demonstrated as a function of m for linear, quadratic and exponential forms of $K(x)$ in figures 7(a), 7(b) and 7(c), respectively. The base flow is stable in the region lying below the curves of $\tilde{R}_{Dc}$ (figure 7a) wherein the value of c_i is always negative, but in the region above these curves the flow is unstable as there exists at least one positive value of c_i. An evident feature that follows from figure 7(a) is that the magnitude of m plays a crucial role on the stability of fluid flow. The flow is found to be always stable in a certain range of values of m as the perturbations ensure a negative growth rate: $-0.3754 < m < 0.3754$, $-0.2498 < m < \infty$ and $-0.5695 < m < 0.5695$ for linear, quadratic and exponential forms of $K(x)$, respectively. This is because the effect of horizontal heterogeneity of the permeability may not be strong enough to induce instability. However, there exists a self-excited mode of disturbances beyond these ranges of values of m and the flow becomes unstable; a result of the contrast observed in the case of constant permeability (Gill 1969). We note that the curves of $\tilde{R}_{Dc}$ decrease rapidly for linear and quadratic forms of $K(x)$ with increasing $|m|(\leq 0.99)$ and

Figure 4. Growth rate c_i versus wavenumber a for different values of (*a*) $\tilde{R}_D$ with $m = \pm 0.2$, (*b*) $\tilde{R}_D$ with $m = -0.3$ and (*c*) m with $\tilde{R}_D = 10^5$ for a quadratic heterogeneity of the permeability.

$-m(\leq 0.94)$, respectively. For these two cases, the curves, after bending a little upward, end at some point after which no more critical values exist as $c_i > 0$. For an exponential form of $K(x)$, the curve of $\tilde{R}_{Dc}$ decreases suddenly and reaches its minimum value at $|m| = 1.9$. In other words, there exists a finite range of values of $|m|$ in which the flow is destabilizing. While for values of $|m| > 1.9$, $\tilde{R}_{Dc}$ increases gradually (i.e. flow is stabilizing) and finally reaches an asymptotic value $86.92|m|$ for sufficiently large values of $|m|$. It is thus evident that the results are independent of the sign of m both for linear and exponential heterogeneities of the permeability, as implied by the symmetry formulated by (3.7*a*,*b*) and the results tabulated in table 3 also confirm this. From the foregoing results, it is evident that the stability of the base flow can be controlled by the permeability functions.

The variation of the corresponding critical wavenumber a_c is shown as a function of m in figure 7(*b*). For linear and quadratically varying permeability models, a_c increases sharply at the beginning and then starts decreasing with increasing $|m|$ and $-m$, respectively. For the permeability model varying exponentially, a_c increases initially then starts decreasing and again increases steadily for values of $|m| \geq 2.21$, and eventually attains the value $a_c = 0.5207|m|$ for sufficiently large values of $|m|$. Thus the size of the convection
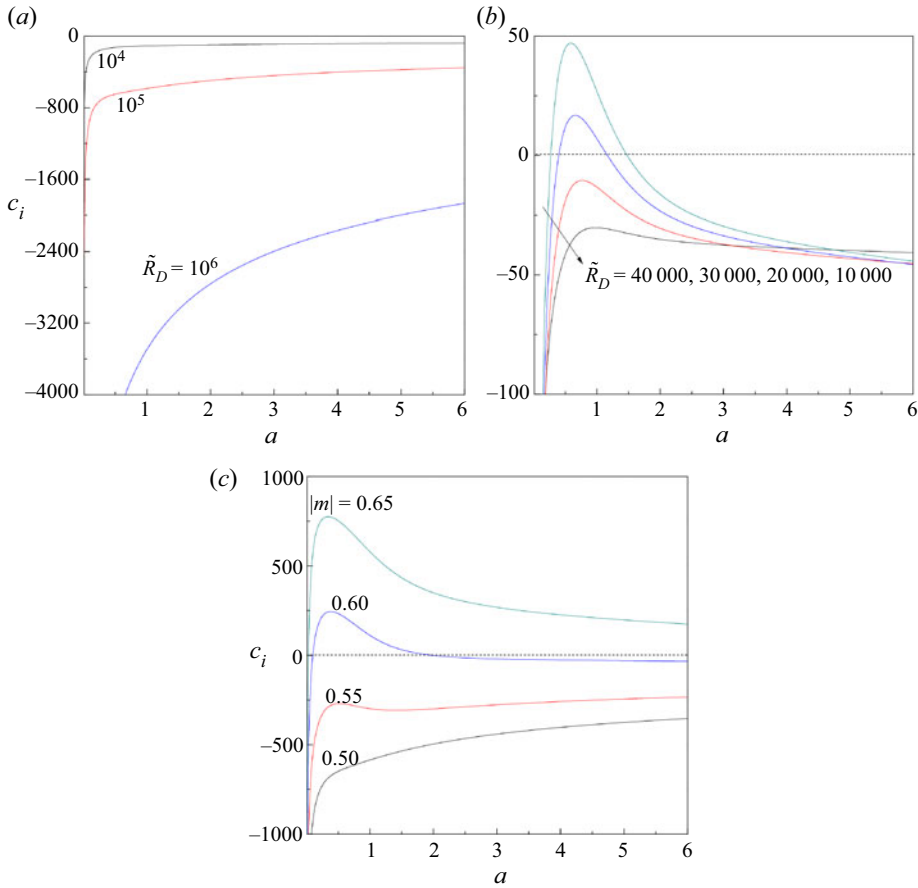
943 A20-15

Figure 5. Growth rate c_i versus wavenumber a for different values of (a) $\tilde{R}_D$ with $|m| = 0.5$, (b) $\tilde{R}_D$ with $|m| = 0.6$ and (c) $|m|$ with $\tilde{R}_D = 10^5$ for an exponential heterogeneity of the permeability.

cell diminishes as $|m|$ takes larger values. The critical wave speed c_c is found to increase steadily with decreasing $-m$ but decreases with decreasing m for both linear and exponential permeability models (figure 7c). In these cases, the sign of c_c becomes negative when m is positive and *vice versa* but its modulus does not change. Thus cells move up the vertical porous slab when the solutions correspond to $c_c < 0$ and move down when $c_c > 0$. For a quadratic form of permeability, $\pm c_c$ exists for each value of $-m$, indicating wave disturbances travelling vertically both upward and downward with equal speed. This is because, if $c = c_1 + ic_2$ is an eigenvalue of $B^{-1}A$ for a given value of $-m$ and the wavenumber a, then $c = -c_1 + ic_2$ is also an eigenvalue of $B^{-1}A$ as ψ_b is an even function of x.

8. Conclusions

An analysis of the stability of natural convection has been carried out for a vertical porous slab considering linear, quadratic and exponential heterogeneities of the permeability. The boundaries of the slab are impermeable and kept at constant but different temperatures. The stability eigenvalue problem has been formulated and solved numerically by employing the Chebyshev collocation method. The neutral stability condition and the
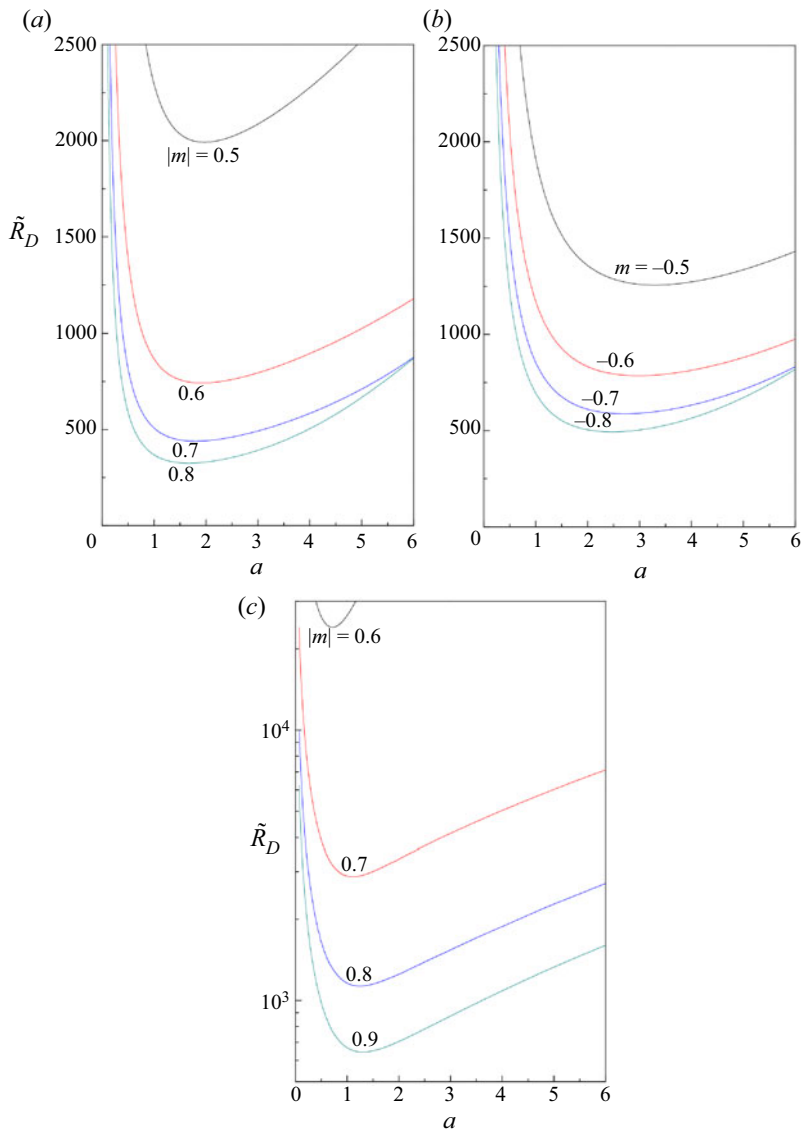
943 A20-16

Figure 6. Neutral stability curves in the $(a, \tilde{R}_D)$-plane for different values of the variable permeability constant m and for the heterogeneity models of (*a*) linear, (*b*) quadratic and (*c*) exponential.

critical Darcy–Rayleigh number for different heterogeneity models are determined. The suitable symmetries of the stability eigenvalue problem for linear and exponential models of heterogeneity have been established, allowing us to gather information on the regime $m < 0$ from the results of $m > 0$. Some of the important results of this analysis can be outlined as follows.

(i) Gill's proof of stability, for the case of constant permeability, has been restated. It has been evidenced that this proof turns out to be ineffective if heterogeneity in permeability exists.

(ii) The heterogeneities of the permeability change the basic flow dramatically and also make the base flow unstable depending on the heterogeneity model as well as the
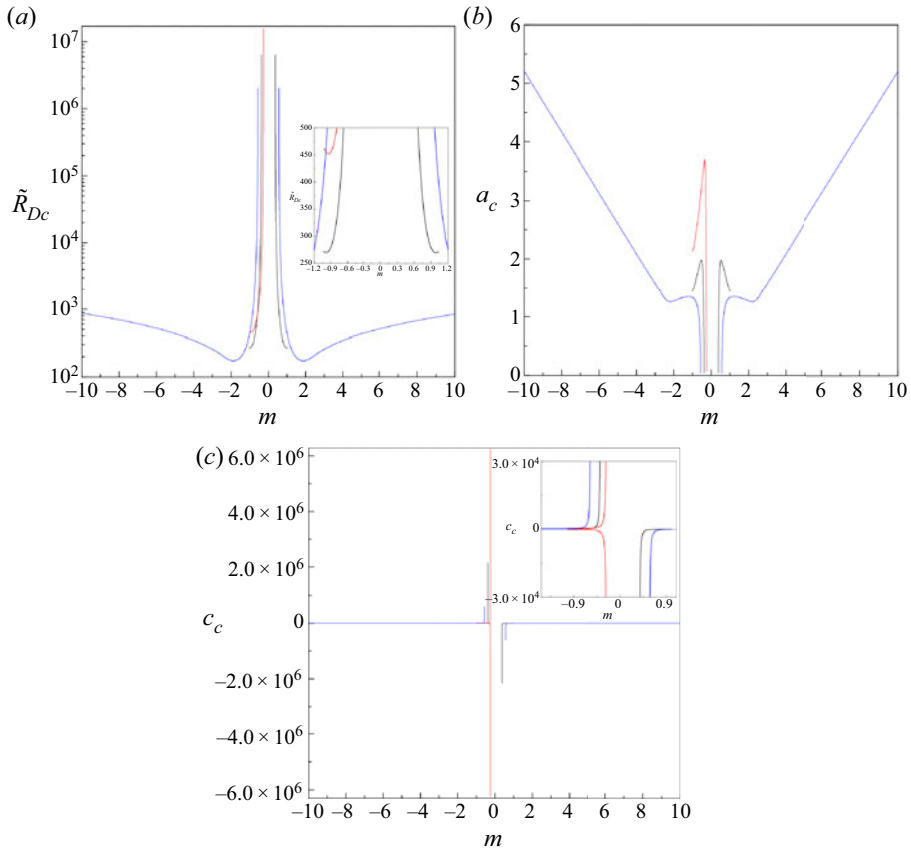
Figure 7. Plots of (*a*) $\tilde{R}_{Dc}$, (*b*) a_c and (*c*) c_c versus m for different heterogeneity models of permeability: linear (black), quadratic (red) and exponential (blue).

variable permeability constant m. In the limit of vanishingly small m, the results for constant permeability are retrieved.

(iii) For quadratic form of heterogeneity, the base flow remains stable for all positive values of m and the instability occurs only for negative values of m.

(iv) For linear heterogeneity of the permeability, the value of $\tilde{R}_{Dc}$ decreases in the range $0.3754 \leq |m| \leq 0.99$ but it pinches upward slightly in a smaller range of $|m| > 0.99$, after which the flow remains unstable. A similar behaviour is noticed for the permeability varying quadratically but only for negative values of m.

(v) For the exponentially varying permeability, the base flow becomes destabilized by manifesting itself as a minimum in the $(m, \tilde{R}_{Dc})$-plane in a parametric space $0.5695 \leq |m| \leq 1.9$ and instead stabilizes for $|m| > 1.9$. Also, $\tilde{R}_{Dc}$ and a_c attain asymptotic values $86.92|m|$ and $0.5207|m|$, respectively, at sufficiently large values of $|m|$.

(vi) The instability sets in always via a travelling-wave mode for all heterogeneity models of the permeability.

Finally, considering the novelty of the present study, we believe that additional research is needed to better understand the stability of this class of basic states. In particular, the transition to absolute instability, the dynamics of spatial modes and the nonlinear development of the disturbances are possible tasks for future work. One of

			Linear heterogeneity of the permeability				
m	$\tilde{R}_{Dc}$	a_c	c_c	m	$\tilde{R}_{Dc}$	a_c	c_c
0.4	32425.8937	1.1278	-10467.9340	-0.4	32425.8937	1.1278	10467.9340
0.5	1991.9150	1.9703	-560.7646	-0.5	1991.9150	1.9703	560.7646
0.6	742.2006	1.9197	-188.8948	-0.6	742.2006	1.9197	188.8948
0.8	324.7667	1.6677	-72.8429	-0.8	324.7667	1.6677	72.8429
			Exponential heterogeneity of the permeability				
m	$\tilde{R}_{Dc}$	a_c	c_c	m	$\tilde{R}_{Dc}$	a_c	c_c
0.6	24025.2370	0.7147	-6893.5068	-0.6	24025.2370	0.7147	6893.5068
0.8	1130.7046	1.2448	-267.5941	-0.8	1130.7046	1.2448	267.5941
2	175.1176	1.2698	-25.9326	-2	175.1176	1.2698	25.9326
5	434.4397	2.6039	-56.7243	-5	434.4397	2.6039	56.7243

Table 3. Critical values of $(\tilde{R}_D, a, c)$ for various selected parametric values.

the most intriguing breakthroughs of this study is the introduction of a model for permeable/partially permeable boundary conditions. Also, one may extend the present problem by considering the time-dependent velocity term in the momentum equation and also horizontal heterogeneity in thermal conductivity.

Author ORCIDs.
 B.M. Shankar https://orcid.org/0000-0001-8194-537X;
 I.S. Shivakumara https://orcid.org/0000-0001-9035-8900.

Appendix A

The Galerkin method has been employed alternatively to solve the resulting eigenvalue problem constituted by (4.3)–(4.5). Accordingly, $\Psi(x)$ and $\Theta(x)$ are expanded in a series of basis functions

$$\Psi(x) = \sum_{n=0}^{N} a_n \xi_n(x), \quad \Theta(x) = \sum_{n=0}^{N} b_n \xi_n(x), \tag{A1a,b}$$

where a_n and b_n are constants and the basis functions $\xi_n(x)$ are represented in terms of Legendre polynomials $P_n(x)$ satisfying the boundary conditions in the form

$$\xi_n(x) = (1 - x^2)P_n(x). \tag{A2}$$

Equation (A1a,b) is substituted back into (4.3) and (4.4), and the resulting momentum and heat transport equations are multiplied by $\xi_m(x)$ and integrated by parts with respect to

x between -1 and 1. This procedure gives two simultaneous algebraic equations governing the coefficients a_n and b_n, which can be written in the matrix form

$$\boldsymbol{AX} = c\boldsymbol{BX}, \tag{A3}$$

where

$$\boldsymbol{A} = \begin{pmatrix} C_{mn} & D_{mn} \\ E_{mn} & F_{mn} \end{pmatrix}; \quad \boldsymbol{B} = \begin{pmatrix} G_{mn} & H_{mn} \\ I_{mn} & J_{mn} \end{pmatrix}; \quad \boldsymbol{X} = \begin{pmatrix} a_n \\ b_n \end{pmatrix}. \tag{A4a–c}$$

The coefficients C_{mn}–J_{mn} involve the inner products of the basis functions given by

$$C_{mn} = \left\langle \frac{1}{K(x)}(\xi_m \xi''_n + a^2 \xi_m \xi_n) \right\rangle - \left\langle \frac{K'(x)}{[K(x)]^2} \xi_m \xi'_n \right\rangle,$$

$$D_{mn} = \frac{\tilde{R}_D}{b} \langle \xi_m \xi'_n \rangle, \quad E_{mn} = \frac{ia}{2} \langle \xi_m \xi_n \rangle,$$

$$F_{mn} = -ia \langle \psi'_b \xi_m \xi_n \rangle + \langle \xi_m \xi''_n + a^2 \xi_m \xi_n \rangle, \quad G_{mn} \approx 0,$$

$$H_{mn} = 0, \quad I_{mn} = 0, \quad J_{mn} = ia \langle \xi_m \xi_n \rangle, \tag{A5}$$

where the inner product is defined as $\langle \cdots \rangle = \int_{-1}^{1} (\cdots) \, dx$. Equation (A3) is solved numerically, as explained in § 6, to obtain the critical stability parameters.

REFERENCES

BARLETTA, A. 2015 A proof that convection in a porous vertical slab may be unstable. *J. Fluid Mech.* **770**, 273–288.

BARLETTA, A. 2016 Instability of stationary two-dimensional mixed convection across a vertical porous layer. *Phys. Fluids* **28**, 014101.

BARLETTA, A. & CELLI, M. 2017 Instability of parallel buoyant flow in a vertical porous layer with an internal heat source. *Intl J. Heat Mass Transfer* **111**, 1063–1070.

BARLETTA, A. & CELLI, M. 2021 Anisotropy and the onset of the thermoconvective instability in a vertical porous layer. *J. Heat Transfer* **143**, 102601.

BARLETTA, A., CELLI, M. & KUZNETSOV, A. 2012 Heterogeneity and onset of instability in Darcy's flow with a prescribed horizontal temperature gradient. *J. Heat Transfer* **134**, 042602.

BARLETTA, A., CELLI, M. & OUARZAZI, M.N. 2017 Unstable buoyant flow in a vertical porous layer with convective boundary conditions. *Intl J. Therm. Sci.* **120**, 427–436.

BARLETTA, A. & DE B. ALVES, L.S. 2014 On Gill's stability problem for non-Newtonian Darcy's flow. *Intl J. Heat Mass Transfer* **79**, 759–768.

BARLETTA, A. & NIELD, D.A. 2012 On Hadley flow in a porous layer with vertical heterogeneity. *J. Fluid Mech.* **710**, 304–323.

BENENATI, R.F. & BROSILOW, C.B. 1962 Void fraction distribution in beds of spheres. *AIChE J.* **8**, 359–361.

BENHAM, G.P., BICKLE, M.J. & NEUFELD, J.A. 2021 Upscaling multiphase viscous-to-capillary transitions in heterogeneous porous media. *J. Fluid Mech.* **911**, A59.

BRAESTER, C. & VADASZ, P. 1993 The effect of a weak heterogeneity of a porous medium on natural convection. *J. Fluid Mech.* **254**, 345–362.

CELLI, M., BARLETTA, A. & REES, D.A.S. 2017 Local thermal non-equilibrium analysis of the instability in a vertical porous slab with permeable sidewalls. *Transp. Porous Med.* **119**, 539–553.

DAMENE, D., ALLOUI, Z., ALLOUI, I. & VASSEUR, P. 2021 Variable permeability effects on natural convection in a vertical porous layer with uniform heat flux from the side. *Transp. Porous Med.* **137**, 287–306.

FAJRAOUI, N., FAHS, M., YOUNES, A. & SUDRET, B. 2017 Analyzing natural convection in porous enclosure with polynomial chaos expansions: effect of thermal dispersion, anisotropic permeability and heterogeneity. *Intl J. Heat Mass Transfer* **115**, 205–224.

FLAVIN, J.N. & RIONERO, S. 1999 Nonlinear stability for a thermofluid in a vertical porous slab. *Contin. Mech. Thermodyn.* **11**, 173–179.

GILL, A.E. 1969 A proof that convection in a porous vertical slab is stable. *J. Fluid Mech.* **35**, 545–547.

NAVEEN, S.B., SHANKAR, B.M. & SHIVAKUMARA, I.S. 2020 Finite Darcy-Prandtl number and maximum density effects on Gill's stability problem. *J. Heat Transfer* **142**, 102601.

NGUYEN, V.T., GRAF, T. & GUEVARA MOREL, C.R. 2016 Free thermal convection in heterogeneous porous media. *Geothermics* **64**, 152–162.

NIELD, D.A. 2008 General heterogeneity effects on the onset of convection in a porous medium. In *Emerging Topics in Heat and Mass Transfer in Porous Media* (ed. P. Vadasz), pp. 63–84. Springer.

NIELD, D.A. & BEJAN, A. 2017 *Convection in Porous Media*, 5th edn. Springer International Publishing.

NIELD, D.A. & KUZNETSOV, A.V. 2007 The effect of combined vertical and horizontal heterogeneity on the onset of convection in a bidisperse porous medium. *Intl J. Heat Mass Transfer* **50**, 3329–3339.

REES, D.A.S. 1988 The stability of Prandtl–Darcy convection in a vertical porous layer. *Intl J. Heat Mass Transfer* **31**, 1529–1534.

REES, D.A.S. 2011 The effect of local thermal nonequilibrium on the stability of convection in a vertical porous channel. *Transp. Porous Med.* **87**, 459–464.

REES, D.A.S. & POP, I. 2000 Vertical free convection in a porous medium with variable permeability effects. *Intl J. Heat Mass Transfer* **43**, 2565–2571.

RIONERO, S. 2011 Onset of convection in porous materials with vertically stratified porosity. *Acta Mech.* **222**, 261–272.

ROBLEE, L.H.S., BAIRD, R.M. & TIERNEY, J.W. 1958 Radial porosity variations in packed beds. *AIChE J.* **4**, 460–464.

SALIBINDLA, A.K.R., SUBEDI, R., SHEN, V.C., MASUK, A.U.M. & NI, R. 2018 Dissolution-driven convection in a heterogeneous porous medium. *J. Fluid Mech.* **857**, 61–79.

SCHWARTZ, C.E. & SMITH, J.M. 1953 Flow distribution in packed beds. *Ind. Engng Chem.* **45**, 1209–1218.

SCOTT, N.L. & STRAUGHAN, B. 2013 A nonlinear stability analysis of convection in a porous vertical channel including local thermal nonequilibrium. *J. Math. Fluid Mech.* **15**, 171–178.

SHAFABAKHSH, P., FAHS, M., ATAIE-ASHTIANI, B. & SIMMONS, C.T. 2019 Unstable density-driven flow in fractured porous media: the fractured elder problem. *Fluids* **4**, 168.

SHANKAR, B.M., KUMAR, J. & SHIVAKUMARA, I.S. 2017 Stability of natural convection in a vertical layer of Brinkman porous medium. *Acta Mech.* **228**, 1–19.

SHANKAR, B.M., KUMAR, J. & SHIVAKUMARA, I.S. 2020 Benchmark solution for the hydrodynamic stability of plane porous-Couette flow. *Phys. Fluids* **32**, 104101.

SHANKAR, B.M., KUMAR, J. & SHIVAKUMARA, I.S. 2021 Numerical investigation of the stability of mixed convection in a differentially heated vertical porous slab. *Appl. Maths Comput.* **389**, 125486.

SHANKAR, B.M., NAVEEN, S.B. & SHIVAKUMARA, I.S. 2022 Stability of double-diffusive natural convection in a vertical porous layer. *Transp. Porous Med.* **141**, 87–105.

SHANKAR, B.M. & SHIVAKUMARA, I.S. 2017 On the stability of natural convection in a porous vertical slab saturated with an Oldroyd-B fluid. *Theor. Comput. Fluid Dyn.* **31**, 221–231.

SHANKAR, B.M. & SHIVAKUMARA, I.S. 2020 Stability of porous-Poiseuille flow with uniform vertical throughflow: high accurate solution. *Phys. Fluids* **32**, 044101.

SHANKAR, B.M. & SHIVAKUMARA, I.S. 2021 Stability of Poiseuille flow in an anisotropic porous layer with oblique principal axes: more accurate solution. *Z. Angew. Math. Mech.* **101**, e201900264.

SHANKAR, B.M., SHIVAKUMARA, I.S. & NAVEEN, S.B. 2021 Density maximum and finite Darcy-Prandtl number outlooks on Gill's stability problem subject to a lack of thermal equilibrium. *Phys. Fluids* **33**, 124108.

STRAUGHAN, B. 1988 A nonlinear analysis of convection in a porous vertical slab. *Geophys. Astrophys. Fluid Dyn.* **42**, 269–275.

WOLANSKI, E.J. 1973 Convection in a vertical porous slab. *Phys. Fluids* **16**, 2014–2016.